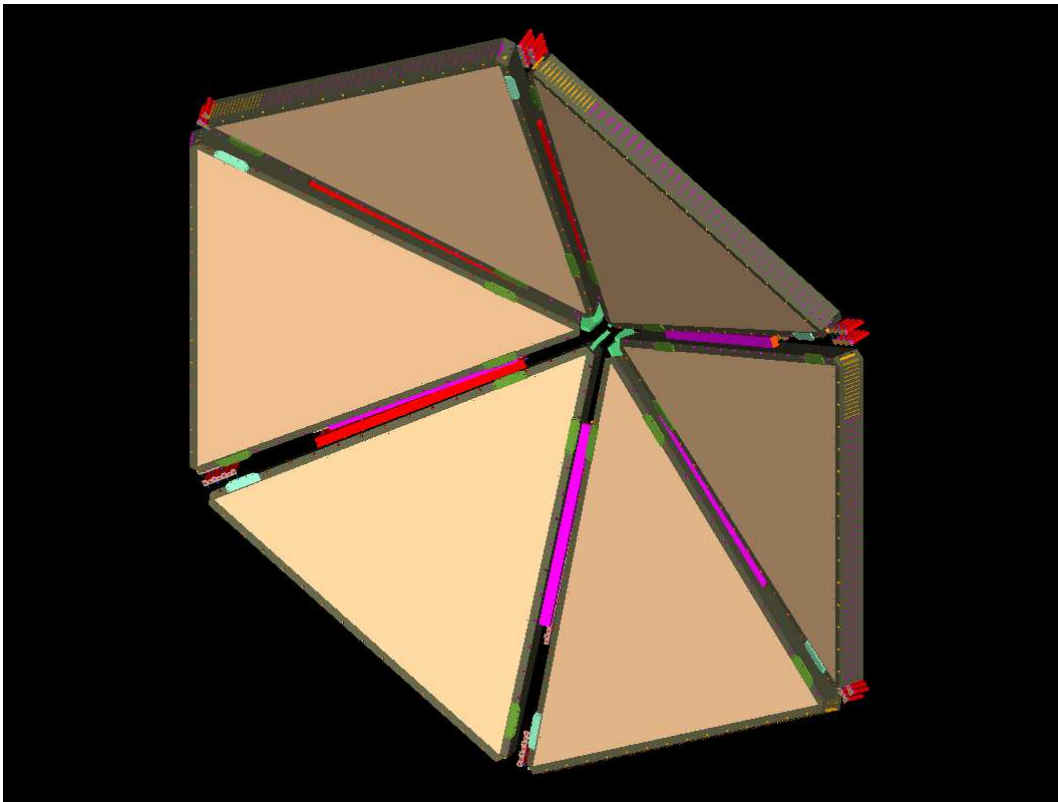# Pre-shower calorimeter for the CLAS12 detector

Version 1.1

Pre-shower calorimeter for the CLAS12 detector

G. Asryan, N. Dashyan, H. Voskanyan

Yerevan Physics Institute, 375036 Yerevan, Armenia

V. Burkert, D. Kashy, S. Stepanyan

Jefferson Lab, Newport News, VA 23606, USA

M. MacCormick, P. Rosier

Institut de Physique Nucleaire d'Orsay, IN2P3, BP 1, 91406 Orsay, France

C. Salgado, M. Khandaker

Norfolk State University, Norfolk VA 23504, USA

K. Hicks

Ohio University, Department of Physics, Athens, OH 45701, USA

K. Giovanetti

James Madison University, Harrisonburg, Virginia 22807, USA

Abstract

The CLAS12 detector package will include the existing electromagnetic calorimeters of the CLAS detector. Calorimeters in CLAS12 will be used primarily for identification of electrons, photons, $\pi^0 \to \gamma\gamma$, and neutrons. At high energies, the existing calorimeters alone will not be able to provide necessary accuracy for energy and position measurements of electromagnetic showers. Therefore, pre-shower calorimeters are proposed to install in front of the existing electromagnetic calorimeters. The pre-shower calorimeter will have similar geometrical design and the readout scheme as the present calorimeters: lead-scintillator sandwich with three stereo readout planes. Proposed pre-shower will be

about 5.5 radiation lengths and will have smaller readout segmentation in the transverse direction than the present calorimeter. Light, produced in the scintillator strips will be transported to a photomultiplier tube via 1 mm diameter wave-length shifting fibers, embedded in the surface of the strip. This addition to the CLAS12 electromagnetic calorimetry in the forward region will allow accurate determination of the shower energy and separation of close clusters from high energy π^0 decays for energies up to 10 GeV.

Contents

1 Overview and Physics Requirements

The primary goal of experiments using the CLAS12 detector at energies up to 11 GeV is the study of the internal nucleon dynamics by accessing the nucleon's generalized parton distributions (GPD's). This is accomplished through the measurement of Deeply Virtual Compton Scattering (DVCS), Deeply Virtual Meson production (DVMP), and single spin asymmetries (SSA). Towards this end, the detector has been tuned for studies of exclusive and semi-inclusive reactions in a wide kinematic range.

The CLAS12 program of experiments goes further than just GPDs and includes experiments such as the space-time characteristics of hadronization. Detection of π^0's is important to complement the measurements of nuclear attenuation seen for charged pions. These experiments depend on the ability to detect π^0's at high momentum.

Copious amounts of high energy particles, both charged and neutral, will be produced at experiments to be done at CLAS12. Electromagnetic calorimeters for the CLAS12 detector should have sufficient radiation length to absorb the full energy of the electromagnetic showers produced by high energy electrons and photons. High energy neutral pions present a challenge as well. Pions decay immediately into two photons with an opening angle that decreases as the π^0 momentum increases. Unless there is sufficient position resolution in the electromagnetic calorimeter of the CLAS12 detector, the two photons from π^0 decay could be seen as a single high-energy photon.

The separation of single high-energy photons from the photons of π^0 decay is very important to the deep virtual Compton scattering (DVCS) experiments which is a major physics program planned for CLAS12. A single high-energy photon is produced in the reaction $ep \to ep\gamma$ and the largest background to this process is from single π^0 production, $ep \to ep\pi^0$. Clearly, good π^0 detection is crucial to the separate these two processes. In addition, direct π^0 production complements the DVCS measurements by accessing GPDs at low and high momentum transfer $|t|$.

Simulations showed that the existing electromagnetic calorimeter (EC) of CLAS [1] will not be able to absorb the full energy of the electromagnetic showers produced by electrons and photons with momentum above 5 GeV/c. The leakage from the back of the calorimeter will diminish the energy resolution, see Fig. 1.a. Simple kinematics of π^0 decay show that above a momentum of 5.5 GeV/c, the opening angle of the decay photons becomes too small to be resolved with the existing EC, at the distance about 6 m from the target. The readout segmentation of EC is only ~ 10 cm. Simulations with the GEANT software for CLAS12

geometry show that these pions would be seen as a single cluster (i.e., one photon) by the event reconstruction software, see Fig. 1.b.
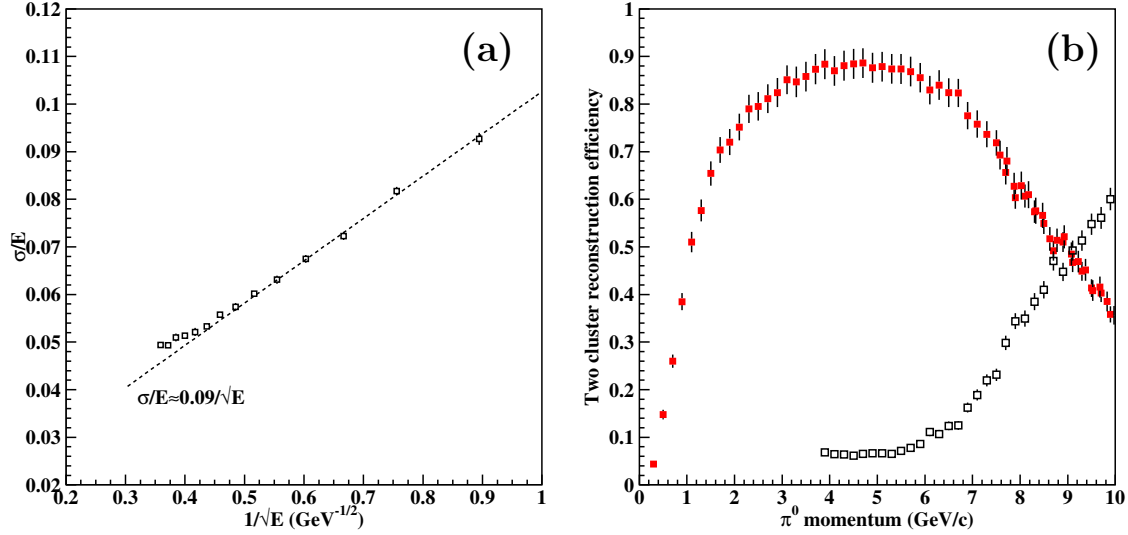

Figure 1: Performance of EC at high energies. a) the energy resolution of EC as a function inverse square root of energy. b) the efficiency of reconstruction of two clusters from π^0 decay photons as a function of pion momentum, filled red squares. The open symbols correspond to the probability that a single cluster is reconstructed with the same energy as the simulated pion.

To reconstruct the energy of high energy showering particles and to separate high energy π^0's and photons, a pre-shower detector (PCAL), with finer granularity, will be built and installed in front of the current EC. The PCAL will have a similar geometry as the current EC. It will be lead-scintillator sandwich with three stereo readout planes. Initial simulations showed [2, 3] that 15 layers of 1 cm thick scintillator layers, segmented into 4.5 cm wide strips, sandwiched between lead sheets of 2.2 mm thickness corresponds to about 5.5 radiation length, will be sufficient to address issues arising at high energies.

In summary, accurate reconstruction of high energy electromagnetic showers and detection of π^0's, and in particular the ability to distinguish single high-energy photons from the two-photon clusters from π^0 decay, is essential to the experimental program using the CLAS12 detector at high energies that will be part of the GPD program. Efficient detection of high momentum π^0's are also needed for a variety of other CLAS12 proposals. The physics dictates the need for a pre-shower calorimeter to be placed in front of the existing EC. Simulations show that good π^0 identification can be obtained with full coverage of the EC front surface. In addition to the improved performance in the reconstruction of electromagnetic shower, the in-

crease of the overall scintillator thickness in the CLAS12 forward electromagnetic calorimeters will increase the detection efficiency for neutrons.

2   Conceptual Design

The design parameters of the PCAL were established using the full GEANT simulations of the PCAL-EC system. As a tool, a modified GEANT simulation computer program for the CLAS detector was used. PCAL was positioned in front of the current EC, see Fig. 2. These studies are described in detail in Refs. [2, 3] and are summarized below. The mechanical design depends on the number of scintillator-lead layers, on the angular coverage of the PCAL, and on the size of the readout segmentation. These parameters were determined by the physics requirements for the detection and identification of high energy electrons, photons, and π^0's via 2γ decay.

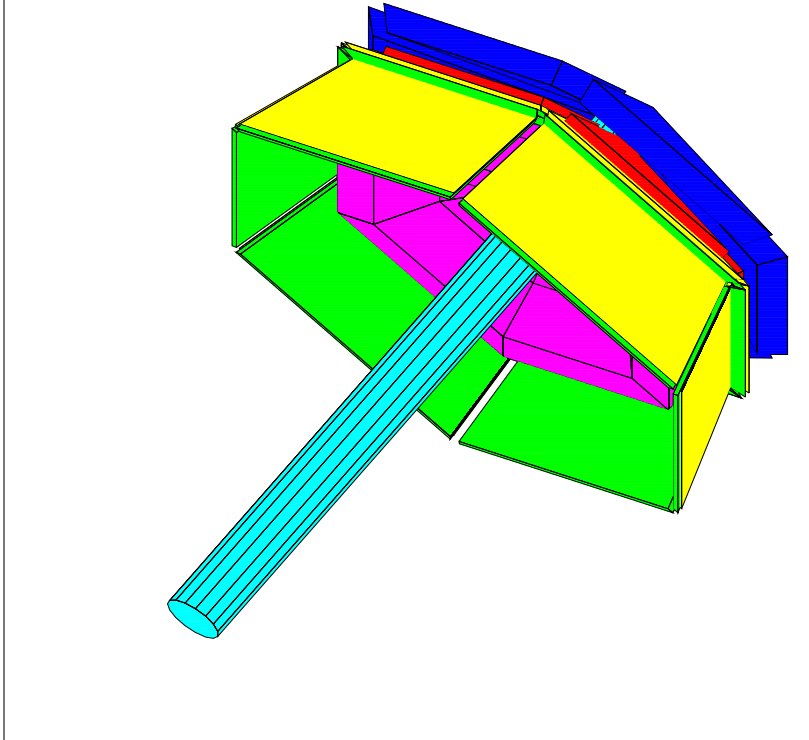Figure 2: Particle ID detector package of the CLAS12 forward region. Low threshold Cherenkov counter is shown in magenta color. Two layers of TOF counters are shown in green and yellow. PCAL is shown in red color and the EC in blue.

Initial simulations were carried out with 15 layers of lead and scintillator (similar to the inner part of the EC), using 35 mm wide segmentation for the scintillator layers, correspond-

ing to about 108 readout channels in each stereo view. Events were generated in a uniform distribution of π^0 and photon events at the target with momenta up to 12 GeV/c. Reconstruction of clusters was done using the standard cluster reconstruction algorithm of the EC, but applied to both PCAL and EC. As shown in Fig. 3, the combined PCAL and EC system retains good energy resolution, $\sigma_E \sim 0.1\sqrt{E}$, and the constant efficiency of two cluster reconstruction up to the highest momenta.
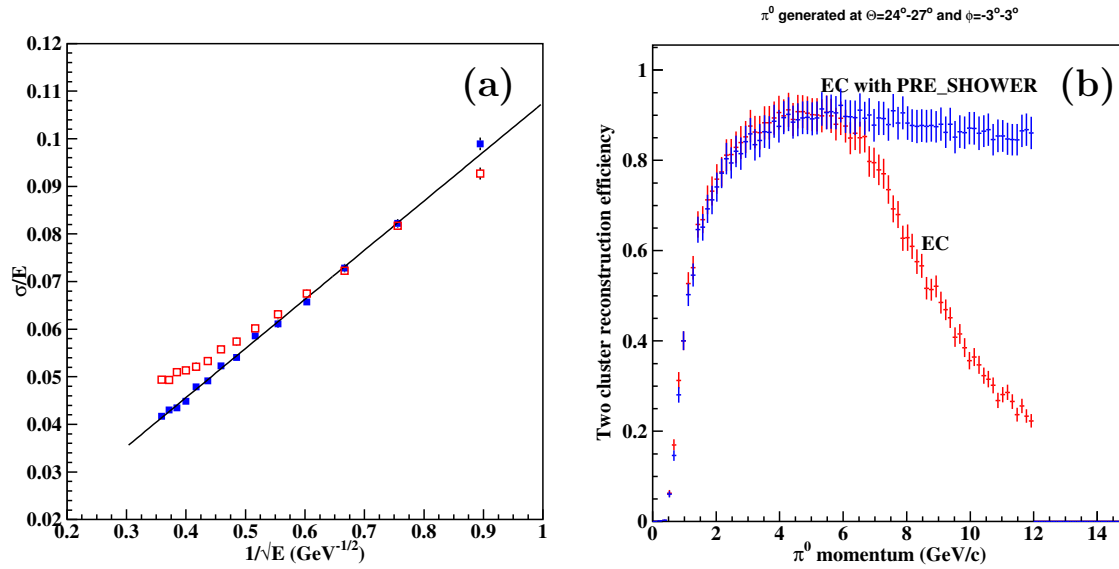

Figure 3: Performance of combined PCAL-EC detector at high energies, shown with blue points. a) the energy resolution of the CLAS12 electromagnetic calorimetry system as a function inverse square root of energy. b) the efficiency of reconstruction of two clusters from π^0 decay photons as a function of pion momentum. Red symbols correspond to EC performance presented in Fig. 1.

Keeping the number of layers at 15, the width of the readout segments (strips) were varied from 35 mm (108 channels) up to 60 mm (65 channels). In Fig. 4a, two cluster reconstruction efficiency is presented for different strip widths. The magenta points correspond to 60 mm strip width, the blue points are for 50 mm segmentation, the green points for 43 mm strip width, and the red points are for 35 mm width. The efficiency decreases with energy for wider strips, but remains reasonably high if the strip size is kept at less than 50 mm.

Other simulations were performed using 9 or 12 layers in the PCAL design, clearly showing a loss of two-cluster reconstruction efficiency. In Fig. 4a two cluster reconstruction efficiency is shown as a function of π^0 momentum for 9 (red), 12 (green), and 15 (blue) layers. Clearly, the 15 layer configuration has the highest efficiency. The reduced efficiency in the other cases are mainly due to insufficient radiation thickness for high energy photons to convert and

deposit sufficient energy for the shower to be detected. Simulations were repeated for the 12-layer case, by doubling the thickness of the first 3 layers of lead. This configuration had a comparable two-cluster reconstruction efficiency as the original 15-layer design, but poorer energy resolution.
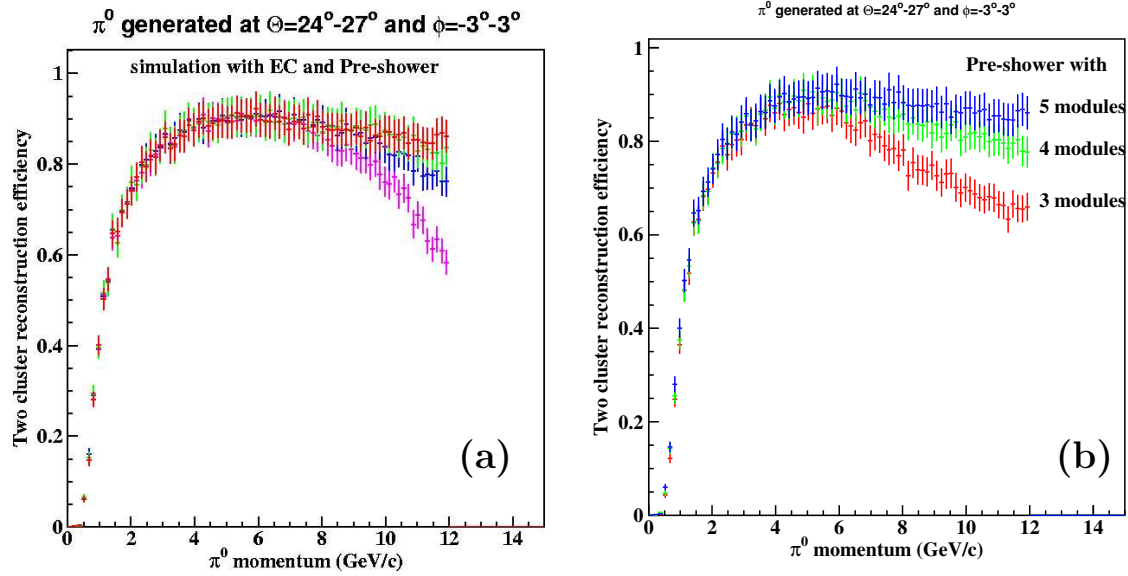

Figure 4: Performance of different configurations of the PCAL. a) the reconstruction efficiency for two clusters from π^0 decay photons as a function of pion momentum, for different readout segmentation. The magenta points correspond to 60 mm strip width, the blue points are for 50 mm segmentation, the green points for 43 mm strip width, and the red points are for 35 mm width. b) the reconstruction efficiency for two clusters for different number of scintillator-lead layers. the red points correspond to 9 layer configuration, the green points are for 12 layers, and the blue points are for 15 layers.

Additional simulations were performed using variable segmentation of the scintillator layers. Keeping constant the total number of readout channels per sector, it was found that the maximum efficiency can be obtained if half of each stereo layers are equipped with 45 mm wide strips and half with 90 mm wide strips (double strip readout). The triangular stereo layers overlap such that there is always a region with 45 mm wide strips in one of the stereo layers, as shown in Fig. 5. There is only a small loss of two-cluster efficiency at the highest momenta for this geometry compared with 45 mm wide strips in all stereo layers, see Fig. 6. It should be noted that at forward angles (short U-strips) where most of the high energy π^0 are produced all three stereo readout views have small readout segmentation.

The proposed design of the PCAL covers the full angular range of the EC. The PCAL has 15 scintillator and 14 lead layers, confined in between two end plates. Variable width
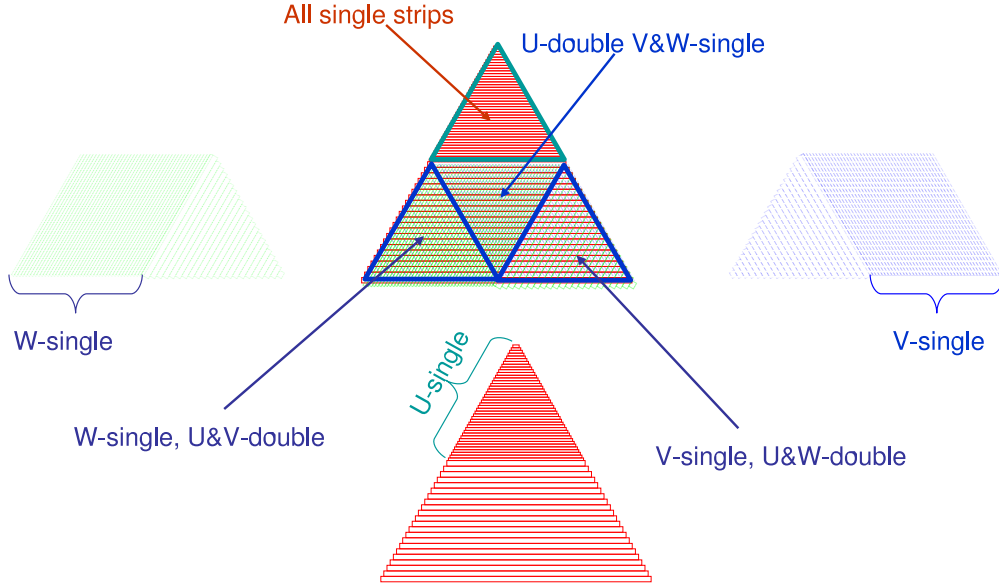
Figure 5: Variable segmentation for different stereo readout planes (U, V, and W). There is always a region with single strip (45 mm segmentation) readout in one of the stereo layers.

of the readout segmentation will be used to minimize the number readout channels while retaining sufficient resolution for the separation of close clusters. It is proposed to use 45 mm segmentation for the short strips in U and for the long strips in V and W stereo readout planes, at least half of the height of the layer. For the remaining part, 90 mm wide segmentation can be used (two strips). The total number of readout channels will be limited to 192 per sector.

3   Mechanical Design

Experience gained in the design and construction followed by 10 years of successful operation of the CLAS electromagnetic calorimeters is the base of the PCAL design. A calorimeter of sampling structure with lead as the radiator and scintillator as the active medium is an economical way of covering a large detection area. Triangular shape of the EC with sides of order of 4.5 meters, matches well the forward angle acceptance of CLAS12. In EC three stereo readout planes were used, segmented into 36 transverse stacks and into two longitudinal parts. The calorimeter showed good performance in terms of energy and position reconstruction of showering particles. The proposed geometry of the PCAL is similar to the geometry of the existing EC, the mechanical design will, however have few essential differences.

The 15 layers of the PCAL will have all the same size, i.e. no pointing geometry as in the
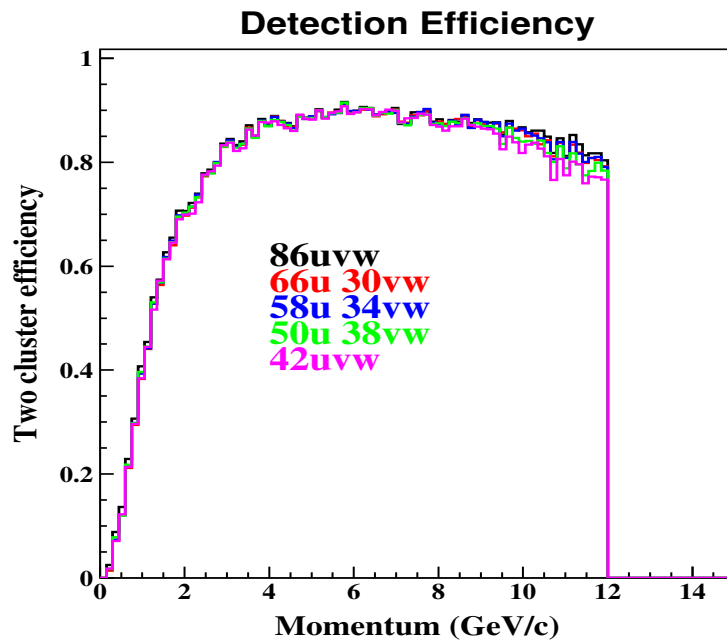
Detection Efficiency

Figure 6: Various combinations of 45 mm and 90 mm readout segmentation. For the black histogram only 45 mm readout is used, amounting to the total of 258 channels per sector. Other histograms correspond to cases when part of the layer was read out in 90 mm segment, keeping the total number of channels to 192 per sector.

EC. This will simplify the design of the container, including individual elements inside, and the assembly process. The triangular box, that will contain scintillators, lead, and support elements, will have 1.5" thick aluminum side walls and two composite end plates. The end plates will be constructed from 2" thick composite foam, sandwiched between 2 mm thick stainless steel sheets connected with aluminum bars. Initial FEA calculations showed that the deflection of plates is less than 1.5 mm in the center in the installed position [6], see Fig. 7.

Light from the scintillator strips will be transported to a photo-detector via wave length shifting fibers embedded in the grooves on the surface of the scintillator strip. There will be no need for optical connections inside the box. This will allow use of simple bars to secure the scintillator and lead layers in place inside the box, see Fig. 8. Spacers will be used to position scintillators and lead sheets inside the box within 1-2 mm tolerances.

Fibers will be brought to the outside via feedthroughs in the side walls. There will be only few feedthroughs, spaced along each side of the triangle. Fibers from several scintillator strips will be routed to a single feedthrough inside the box and will be spread out to the PMT adapters on the outside. There will be shelves mounted along the side walls at the level of the
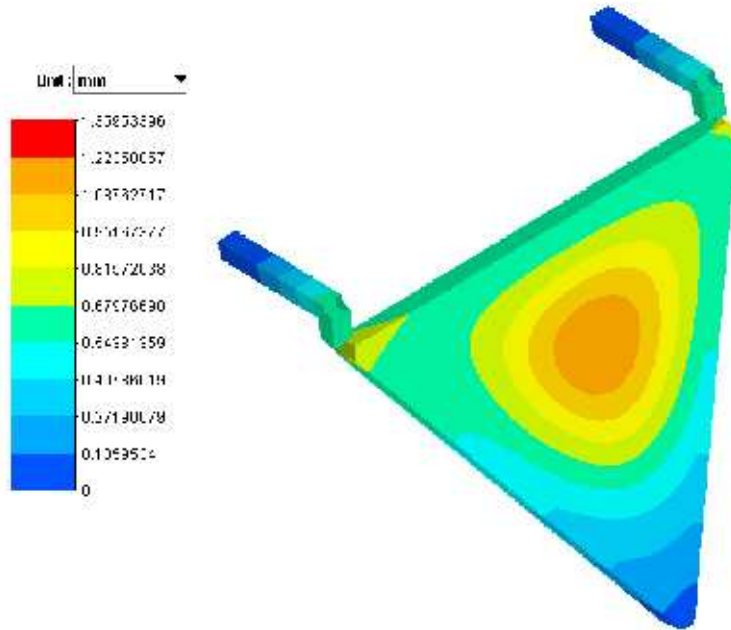
Figure 7: FEA simulation of the end plate deflection in the position of the PCAL in the CLAS12 Sector 2. Maximum deflection with 2" thick Rohacell foam, sandwiched between 2 mm thick stainless steel sheets is less than 1.5 mm.

back plate that will hold adapters for the fiber-PMT connection. The shelves for the two sides will be located in the space between two sectors to allow access to PMTs from the forward carriage (from behind the EC), see Fig. 9. For the side perpendicular to the beam direction, the location and the length of the shelves will be defined by the space free from mounting arms of the low threshold Cherenkov counter. There will be thin aluminum covers along the shelves to make the PCAL container light tight.

4   Signal readout and triggering

The electrical connections of the PCAL PMTs will be as following: dividers for the PCAL PMTs will have HV input and the anode signal as an output. Each PMT will be furnished with separately regulated HV power source. The charge and the time of the anode signals for each PMT will be measured using a flash ADC (FADC) and a multi-hit TDC (MTDC), respectively. The PMT anode signal will be sent to a splitter, about 15 meters of RG58
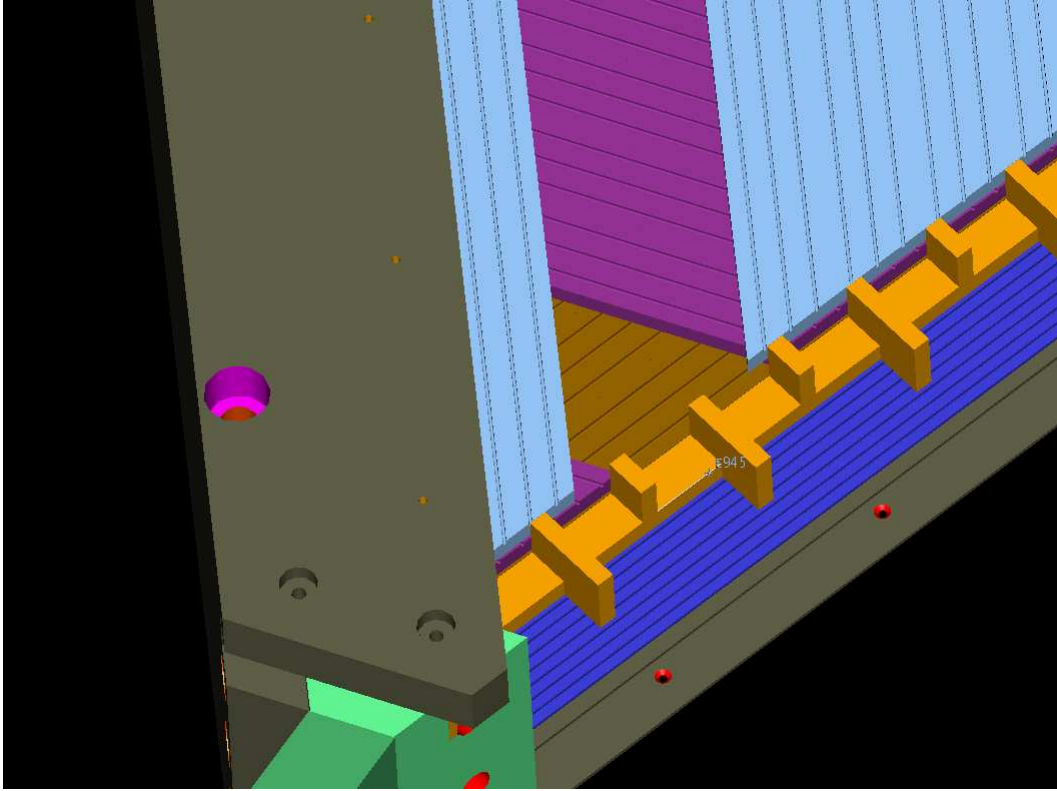
Figure 8: View of the opening of one PCAL sector. Three subsequent scintillator layers have strips oriented parallel to one of sides of the triangle.

cable, with approximately 1 : 3 split. The larger portion of the split, $\sim 75\%$, will be sent to a discriminator input. Outputs from the discriminator will feed the MTDC and a scaler. Second output of the splitter, $\sim 25\%$ of the signal, will go to the FADC. PCAL will be included in the trigger system of the CLAS12. The trigger signals from the PCAL modules will be formed using the fast readout of the FADCs and the FPGA programming of the mainframe controller. This type of trigger organization will allow for more sophisticated and robust trigger configurations compared to the total energy sum trigger configuration.

The energy uniformity of the calorimeter response is one of the important aspects in configuration of trigger systems. The response of the PCAL to electromagnetic energy deposited in the scintillator material across the calorimeter front face depends upon several factors. Assuming that the same amount of energy deposited in the scintillator generates the same amount of light in the scintillating fibers independent of the position across the calorimeter, the light attenuation along in the fiber remains the major factor that determines the PMT response for a given scintillator stack in U, V, and W views. A typical light attenuation for green fibers is $L_0 = 300 - 400$ cm. Depending upon the X-Y position at the calorimeter face,
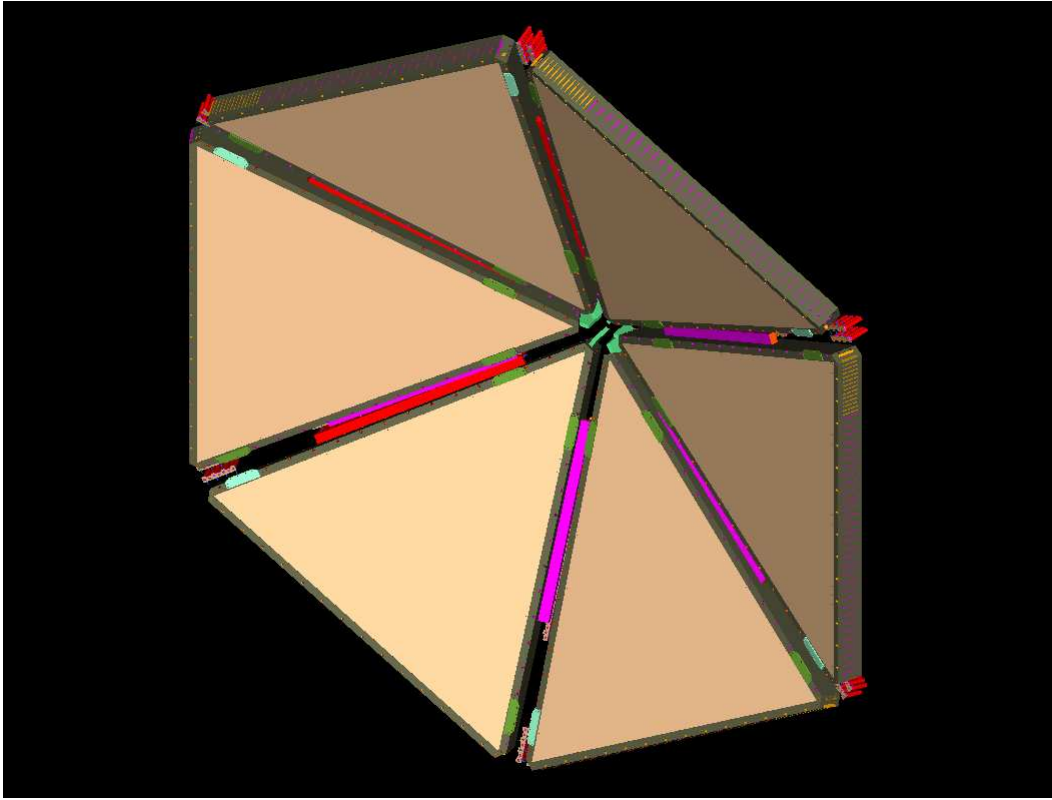
Figure 9: Six sector view of the PCAL. PMTs are shown in red and magenta colors. PMTs for two sides are aligned along the opening between two sectors. On the third side, the side perpendicular to the beam direction, PMTs will occupy the space along the side, where no fixtures for mounting other detectors exist.

the light may travel up to nearly 500 cm before it reaches the photomultiplier. Therefore, the signal may be attenuated by a factor of 4 when reaching the PMT photo-cathode. Therefore the response of individual U, V, or W stacks can vary by large factors making the response highly non-uniform. However, the triangular structure of PCAL with nearly equal side lengths, and with the scintillators oriented approximately 120 degrees relative to each other, reduces this non-uniformity drastically when signal from all strips are added. In fact, in the case of linear attenuation the sum of the signal from the U, V, and W strips is independent of the X-Y position at the calorimeter face. However, in a more realistic case the signal drops like an exponential function of the distance, i.e. $I(L) = I_0 \times exp(-L/L_0)$, where L is the distance along the fiber from where the signal was generated. Adding all signals up will generate significantly higher sums (40%) at the edges and corners of the calorimeter than in the center . While this effect can be corrected in the offline analysis, it could, however, significantly bias the calorimeter response towards lower energy deposition near the edges when used in a total

energy trigger. To avoid this non-uniformity, the PCAL response can be made more uniform by giving lower weight factors to the shorter strips than to the longer strips in the trigger logic using the FADCs and the FPGA programming. The non-uniformity can be reduced to a few percent across the entire PCAL face.

5   Prototyping and Component Testing

The design goals for the PCAL detailed in the previous sections are based on the proposed geometry for CLAS12, the combined performance of the PCAL and the existing EC for CLAS12, and experience gained from the construction followed by 10 years of successful operation of the EC [1]. In addition these factors established the preliminary design.

Principle considerations:

- Comparable geometric coverage for PCAL with respect to the EC,

- Good resolution/calorimetry coverage up to 10 GeV photons and electrons,

- Improved particle identification ability to enhance final state reconstruction at higher energy,

- Information on the longitudinal shower development,

- Fast calorimeter response for use the Level 1 trigger,

- Sufficient position information to resolve $\pi^0 \to \gamma\gamma$,

- Ability to reconstruct the event based on component properties and the readout information,

- Compatibility with the present EC and other CLAS components.

- Mechanical stability,

- Mechanical support viability,

- Constructibility (reasonable facilities, manpower and resources to assemble detectors)

- Reasonable options for testing components in order to establish PCAL operational parameters,

Over ten years of experience has been gained using the EC installed in CLAS. Initially the components were carefully characterized (e.g. scintillator attenuation, light transmission, photo-electron efficiencies). Calibration procedures were developed and continue to be improved to update the relevant properties (e.g. photomultiplier gains and pedestal). This information has been used to construct algorithms for extracting particle id, particle position and particle energy [5]. An EC electronic sum is available as part of the current trigger options for CLAS and has proved to be essential for limiting the amount of recorded data while identifying useful final states. The calorimeter has operated reliably providing critical information on reaction final states and operating with sound performance in terms of maintenance and stability. The mechanical structures for calorimeter movement and support work well. Thus part of PCAL design has been based on the existing EC.

To match the above goals a Pb/scintillator sampling calorimeter with wavelength shifting fiber readout was chosen. Scintillator light readout systems with embedded fibers are well known. This technique was used, for example, in the MINOS FAR detector [8] and many other "tile" calorimeters.

Main design features:

- Triangular shape with sides of order 4.0 m

- Sampling structure with Pb as the radiator and scintillator as the active medium,

  - Lead 2.2 mm (available sheets) [simulation verifies this choice of sheet depth]

  - Scintillator strips

    * scintillator 10 mm longitudinal depth [simulation verifies this choice of sheet depth],

    * Strip width will be important in determining position resolution,

    * Simulation suggests that 4.5 cm width is adequate to reach required position resolution,

    * U,V,W readout

- light readout of the PMT is severely impacted by structure,

- light readout needs to reach several photo-electrons/MeV of deposited energy,

- components need to be combined to reduce the required number of PMTs,

- WLS fiber is the best light readout scheme,

Component testing was primarily focused on finding the components that did not compromise the design goals while minimizing costs. Tests were conducted to find the optimal

- WLS fibers

- photomultiplier tubes

- number of fibers per strip

- grooved scintillators

- glue than binds fibers and scintillator and improves optical properties,

Tests were also designed to characterize combinations of components in terms of the number photo-electrons/MeV and to verify expected attenuation lengths for scintillator and fiber.

For these test measurements, several different types of scintillator, wave shifting fibers (single and multi clad), and photomultiplier tubes, PMTs, were studied, see Table 1. Extruded scintillators from Fermilab (FNAL) and Kharkov, as well as commercial scintillator from EJEN were compared on the basis of light yield and cost. The FNAL and Kharkov strips are grooved during the extrusion by the die[9, 10]¿ whereas the grooves for the ELJEN scintillator were machined by the manufacturer. The grooves provide insets for the WLS fiber. The fibers are held in place by either a UV cured glue or an epoxy. Light absorption by the fiber is influenced by the optical properties of the glue. Preliminary results indicate that an optical epoxy is adequate both in terms of bonding and light transmission. The more expensive UV cured optical glues were used during these tests. The FNAL and Kharkov scintillator strips were coated with a reflective material (1 mm titanium dioxide, excluding the inside surface of grooves) to improve light collection. Tests on the ELJEN scintillator were done with and without an additional aluminized mylar surface. The HAMAMATSU R1450-13 and R6095 PMTs were tested because of their high quantum efficiency at 500 nm. R1450-13 and R6095 PMTs were chosen with QE > 18% and > 16% at 500 nm and studied as possible options. Light yield measurements were done with KURARAY 1.5 mm and 2 mm diameter Y11 fibers to determine the dependence of light yield on the fiber diameter. Finally a sufficient sample of scintillator-WLSF-PMT combinations was studied to determine the optimal combination.

5.1 Setup

Measurements were performed in the semi-clean room in the EEL building at JLAB, using 4 meters long dark box, see Fig.10. The box was instrumented with a moving cart, but for this

PMT	Type	Photo-cathode	# of stages
HAMAMATSU	R7899EG	25 mm	10
	R1450-13	19 mm	10
	R6095	28mm	11
ElectronTubes	9124B	30mm	11
PHOTONIS	XP1912	19mm	10
	XP2802	19mm	10
WLS fibers	Type	Diameter	Cladding
KURARAY	Y11	2mm	Single
	Y11	1.5mm	Single
	Y11	1mm	Single
	Y11	1mm	Multi
BICRON	BC-91A	1mm	Single
	BC-92	1mm	Single
Scintillators	Type	Cross section	# of grooves
ELJEN Tech.	EJ-204	3×1 cm^2	4
	EJ-204	3×1 cm^2	No grooves
FNAL	MINOS	4×1 cm^2	1
Amcrys-Plast, Kharkov		2.6×1 cm^2	2
		2.6×1 cm^2	3

Table 1: Pre-shower readout components used in the test.

set of measurements position dependence of the light yield was not studied and the cart was not used. In Fig.11, a schematic view of the setup is shown. Scintillator strips with fibers were secured inside the box. The trigger PMT was attached directly to the end of the scintillator strip through acrylic light guide. For the scintillator-light guide and the light guide-PMT connections BICRON BC-630 optical grease was used.

WLS fibers were glued inside grooves using Dymax UV curable optical glue OP-52. Fibers were extended about 40 cm from the end of the scintillator in order to connect to the photo-cathode of a test PMT. The test PMT was installed inside a plastic housing, a tube with μ-metal shield inside. The housing tube had two end-cups, one with connectors for HV and

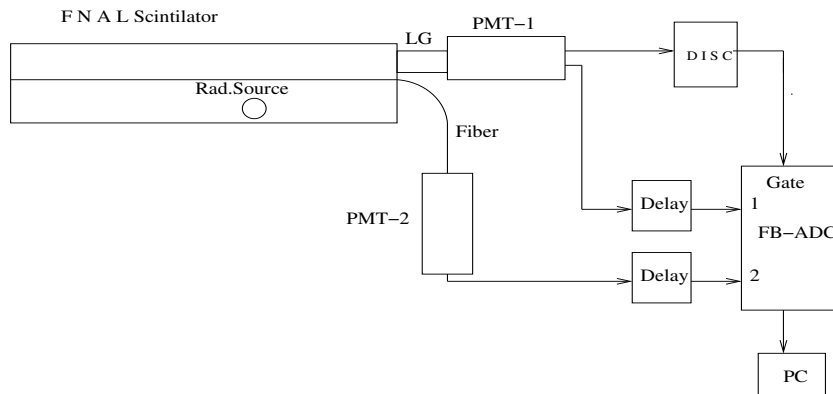Figure 10: Picture of the dark box. Moving cart is mounted on rails

Figure 11: Schematic view of the setup for light yield measurements

signal cables and the another with adapter for the fiber connection [12]. To secure the fiber on the photo-cathode of the test PMT, several plastic adapters were built with thin metallic tubes as inserts. The inner diameter of tubes were chosen to have a tight fit for the fibers. The tubes were aligned along the axis of the PMT and were guiding the fibers in the direction perpendicular to the photo cathode. BICRON EC-630 optical grease was used between the fiber and the photo cathode for good optical contact.

Readout electronics of the system consisted of the LeCroy 1881M ADC and the Philips 704

discriminator. As a gate for the ADC, discriminated pulse from the trigger PMT was used. Signals of the test and the trigger PMTs were delayed and connected to the ADC inputs, see Fig.11. The ADC information was read out using the standard CLAS DAQ software. For each setting, ADC values were written out to a single file. Then the information was copied into HBOOK Ntuple [13]. Analysis of the data were performed in PAW [14].

5.2 Determination of the number of photo-electrons

For the analysis of photo-electron statistics, the method developed in [11] was used. Each ADC spectrum was fitted with a sum of a Poisson distributions, $P_i(n_{pe})$, convoluted with Gaussian functions, $C_i(n_{ch})$. Poisson distributions describe the photo-electron distribution while the Gaussians are used to describe the photomultiplier response. The predicted ADC spectrum for a given average number of photo-electrons will be:

$$A = c \cdot \sum_i P_i(n_{pe}) \times C_i(n_{ch}) \tag{1}$$

$$P_i(n_{pe}) = \frac{n_{pe}^i \cdot e^{-n_{pe}}}{i!} \tag{2}$$

$$C_i(n_{ch}) = \frac{1}{\sigma_1 \cdot \sqrt{i}} \cdot e^{-(\frac{n_{ch}-(a_1+(i-1)\cdot a_0)}{\sigma_1 \cdot \sqrt{2i}})^2} \tag{3}$$

In Eq.(1), summation goes over the possible number of photo-electrons in the spectrum, i. Coefficient c is for the overall normalization, n_{pe} is the average number of photo-electrons. In Eq.(3) n_{ch} is the pedestal subtracted ADC channel number. Parameters a_1 and σ_1 are the position and the standard deviation of the single photo-electron peak in the units of ADC channel. a_0 is the distance between two adjacent photo-electron peaks in the units of ADC channels (not necessary to be equal to a_1). The fit parameters were c, n_{pe}, and a_0.

The parameters a_1 and σ_1 were defined from fits to a single photo-electron distributions for each of the test PMTs. Two examples of single photo-electron peaks are shown in Fig. 12. The left plot shows the response of the PHOTONIS XP2802 PMT as the light intensity is lowered. The right graph shows single photo-electron peak for the HAMAMATSU R6095 PMT. Fig.12.

5.3 Determination of the absolute light yield

Since the measurements were carried out with a β-source, the amount of energy deposited for a given event will vary significantly. Most of the measurements were done with a ^{90}Sr source
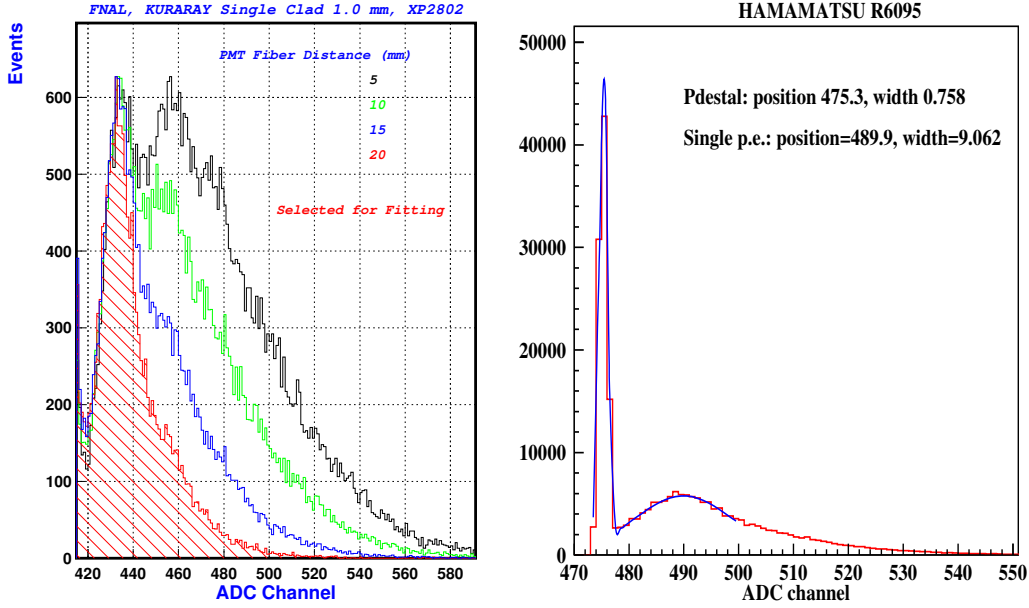
Figure 12: On the left is the ADC distribution of XP2802 PMT corresponding to a few and single photo-electrons. On the right fit to the single photo-electron distribution of the HAMAMATSU R6095 PMT. Fit was done using a sum of two Gaussians, one for the ADC pedestal and the second one is for the single photo-electron distributions.

which provided a 2.3 MeV β based on the decay $^{90}Sr \rightarrow 0.546 MeV\beta^- +^{90}Y \rightarrow 2.28 MeV\beta^-$. Measured responses will however depend on the part of the β spectrum that was selected by the trigger PMT. A typical spectrum is shown in Fig. 13. To reduce systematics due to variation in trigger conditions and to estimate the deposited energy events from the end point of the β spectrum ($\sim$ 2 MeV) were used in the comparisons. The end point was identified by increasing the trigger threshold until the average n_{pe} remained constant. In Fig. 14, fits to the ADC distributions of the HAMAMATSU R7899EG and R6095 PMTs, for different trigger settings (550 to 600) are presented. The dependence of the n_{pe} on the trigger PMT ADC channel is shown in Fig. 15. Closed squares are n_{pe}'s for R7899EG, the open squares are for R6095. As one would expect number of photo-electrons increases with increasing trigger and flattens out at the end.The number of photo-electrons at the end point was taken as a light yield corresponding to a $\sim$ 2 MeV energy deposition.

5.4   Light yield with single fiber readout

Studies of PMT response were performed with the same FNAL scintillator and the single
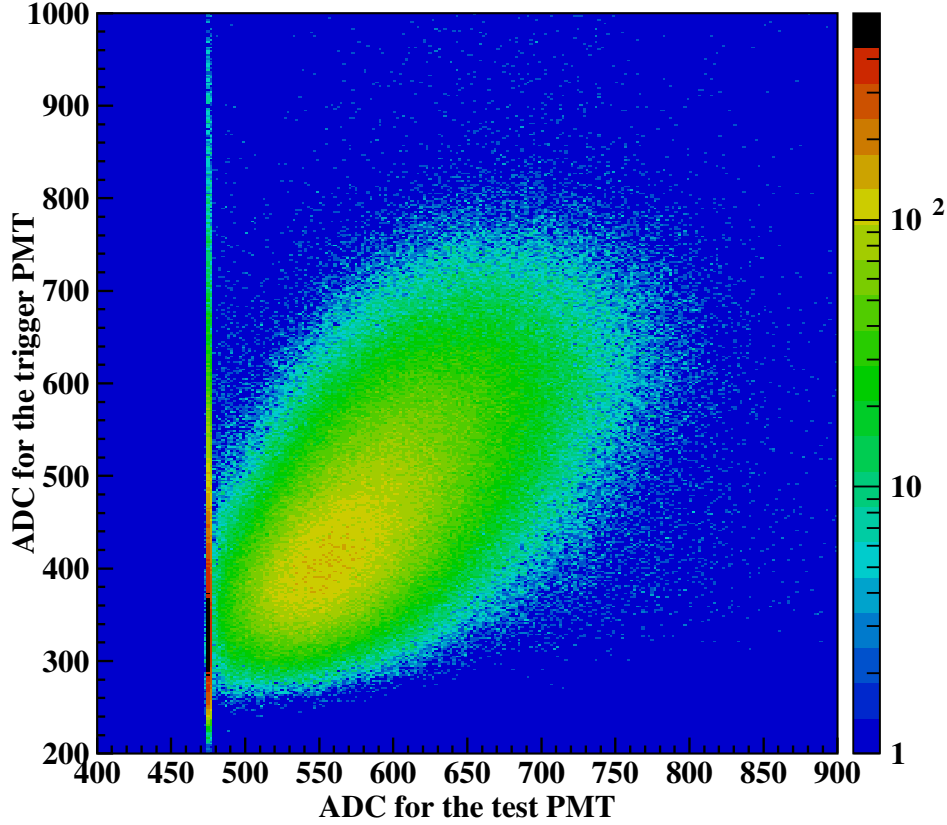
Figure 13: ADC spectra of the trigger and test PMTs. Test PMT ADC distributions for different slices of the trigger PMT ADC were fitted to get photo-electron statistics.

clad 1 mm diameter Y11 WLS fiber (WLSF). Sample results are shown in 16. As stated the response was extrapolated to the end point energy by increasing trigger thresholds. All the fits show the expected flattening at the end of the spectrum. Tabulated yields are based on the end point extrapolation to ~ 2 MeV energy deposition. Table 2.

PMT	R7899EG	R6095	XP2802	R1450	9124B
n_{pe}	10.3	7.6	7.3	6.5	4.7
$\sigma_{n_{pe}}$	0.53	0.57	0.39	0.17	0.14
χ^2	1.7	0.92	1.16	1.23	0.7

Table 2: Number of photo-electrons for different PMTs corresponding to 2 MeV energy deposition in the FNAL extruded scintillator with one groove. Readout with 1mm diameter, single clad Y11 WLS fiber.
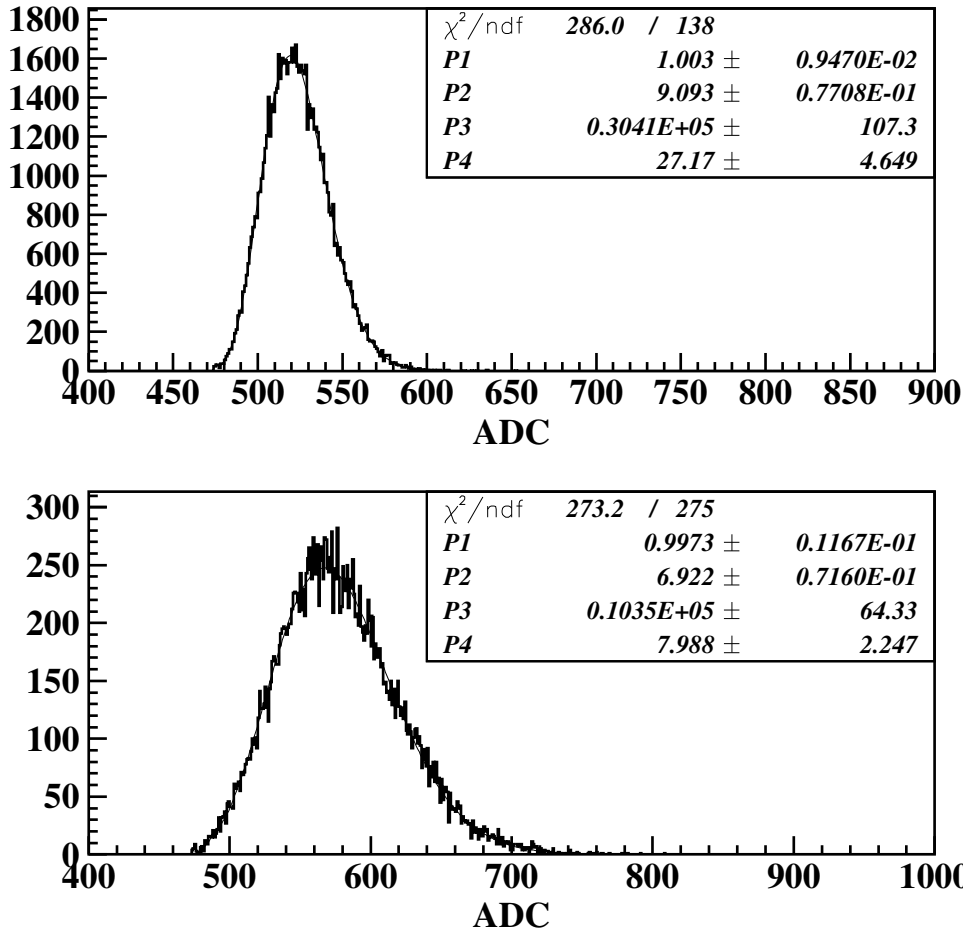
Figure 14: Fit to the ADC spectra of the HAMAMATSU R7899EG and R6095 PMTs with Eq.(2). Spectra correspond to the trigger PMT ADC channels 550 to 600.

The HAMAMATSU R7899EG (green extended photo cathode) has the highest light yield followed by the HAMAMATSU R6095 with $\sim 26\%$ less photo-electrons. The other PMTs, the PHOTONIS XP2902, the ElectronTubes 9124B, and the HAMAMATSU R1450, did not perform as well.

Comparison of the scintillators was done using and R6095 PMT. All the strips had 1 mm, single clad Y11 fiber glued in the groove on the surface of the strip. The EJ204 did not have reflective coating, therefore two measurements with and without wrapping were done for that scintillator. Results are tabulated in Table 3 and are shown in Fig.17. The FNAL extruded scintillator showed the highest light yield.

The candidate WLS fibers were studied. Different type and diameter fibers were glued into the FNAL scintillator strip and the photo-electron statistics was measured with the HAMAMATSU R7899EG PMT. The relative light yield for different fibers is presented in
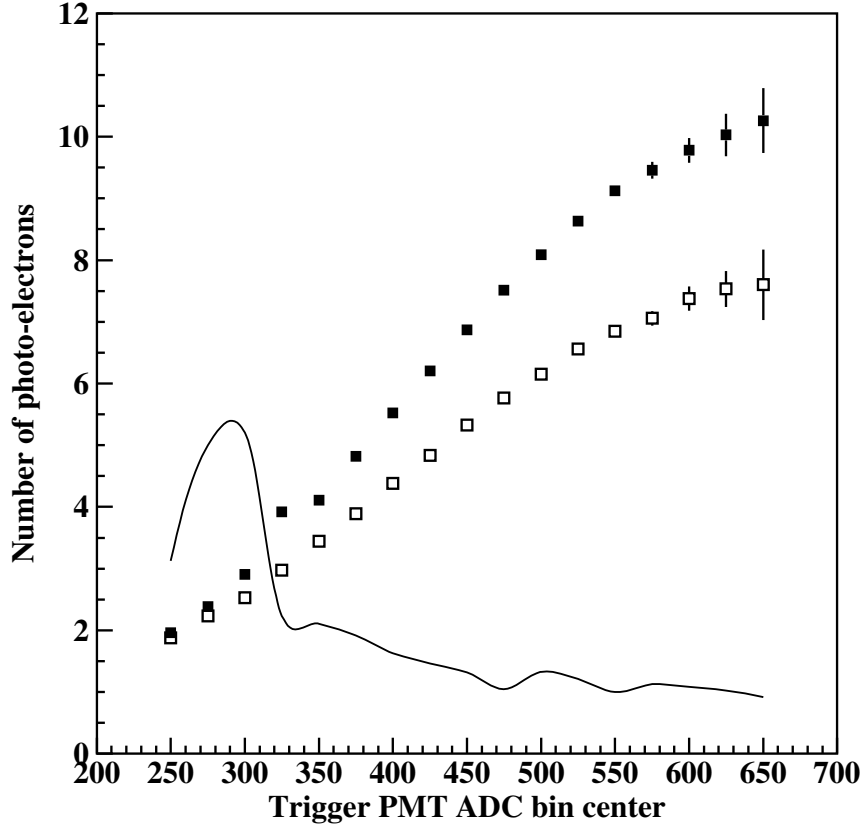
Figure 15: Dependence of the n_{pe} on the trigger PMT ADC channel. On the figure closed squares are the n_{pe} for R7899EG, the open squares are for R6095. The solid line curve is the χ^2 distribution for the fit to the spectra of R7899EG.

	FNAL	ELJEN	ELJEN wrapped	Kharkov
n_{pe}	7.6	2.5	5.7	6.8
$\sigma_{n_{pe}}$	0.57	0.55	0.33	0.23
χ^2	0.92	1.08	1.1	1.02

Table 3: Number of photo-electrons for 2 MeV energy deposition in different scintillator strips. Readout was with 1 mm, single clad Y11 WLS fiber and R6095 PMT.

Fig.18. Light yield for the BICRON G92 fiber is not presented because it was too low (not a surprise since G92 is designed to have fast response time and has small attenuation length).

The number of photo-electrons was observed to increase with the diameter of the fiber. 1.5 mm fiber has $\sim 25\%$ more light than 1 mm diameter fiber and 2 mm fiber has $\sim 40\%$ more
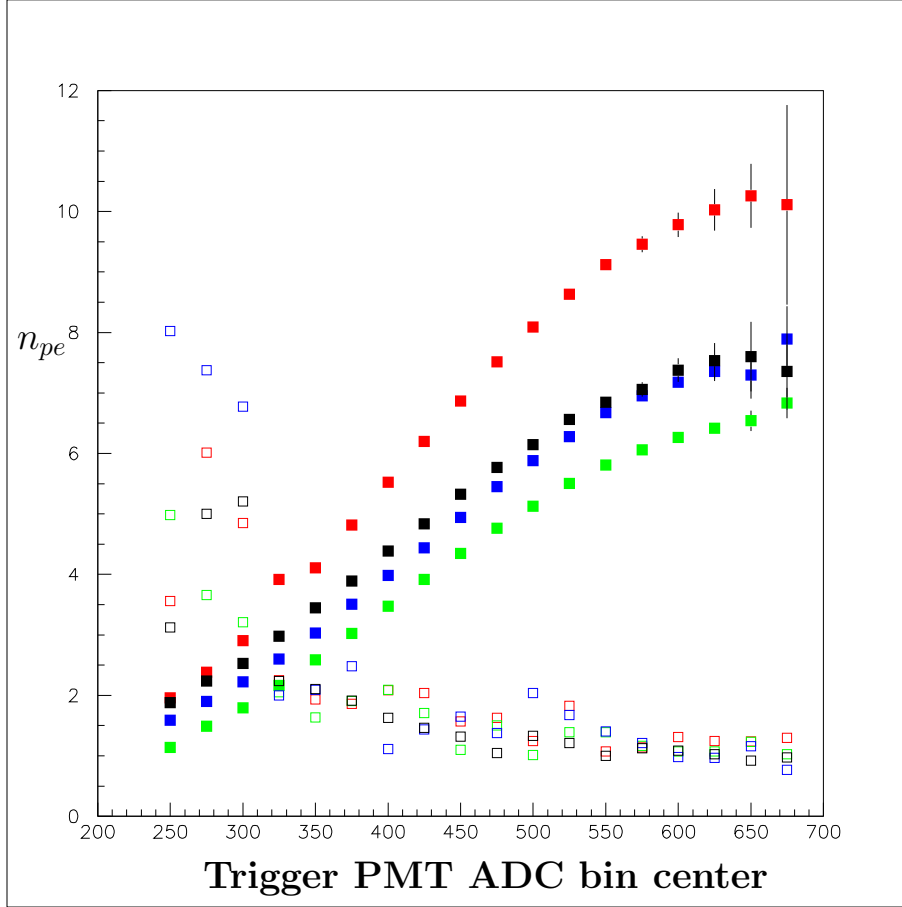
Figure 16: Dependence of the n_{pe}'s on the trigger PMT ADC channel. Closed squares are the n_{pe}'s for R7899EG (red), R6095 (black), XP2802 (blue), and R1450 (green). The open squares the χ^2 distributions for the fits (in the same color codding).

light. The light yield is also higher for multi-clad fiber compare to a single clad by about 20%. Bicron G91A 1 mm diameter, single clad fiber has about 10% less light yield than KURARAY 1.0 mm, single clad Y11.

5.5   More measurements

Additional measurements have been performed to check the systematics of the results. The same scintillator-WLSF-PMT combinations were measured at several settings. Results from different measurements were consistent to within few percent. One of the major sources of the uncertainties is the determination of the single photo-electron peak position and the Gaussian width for a given PMT. Therefore measurements for one PMT but several different voltages
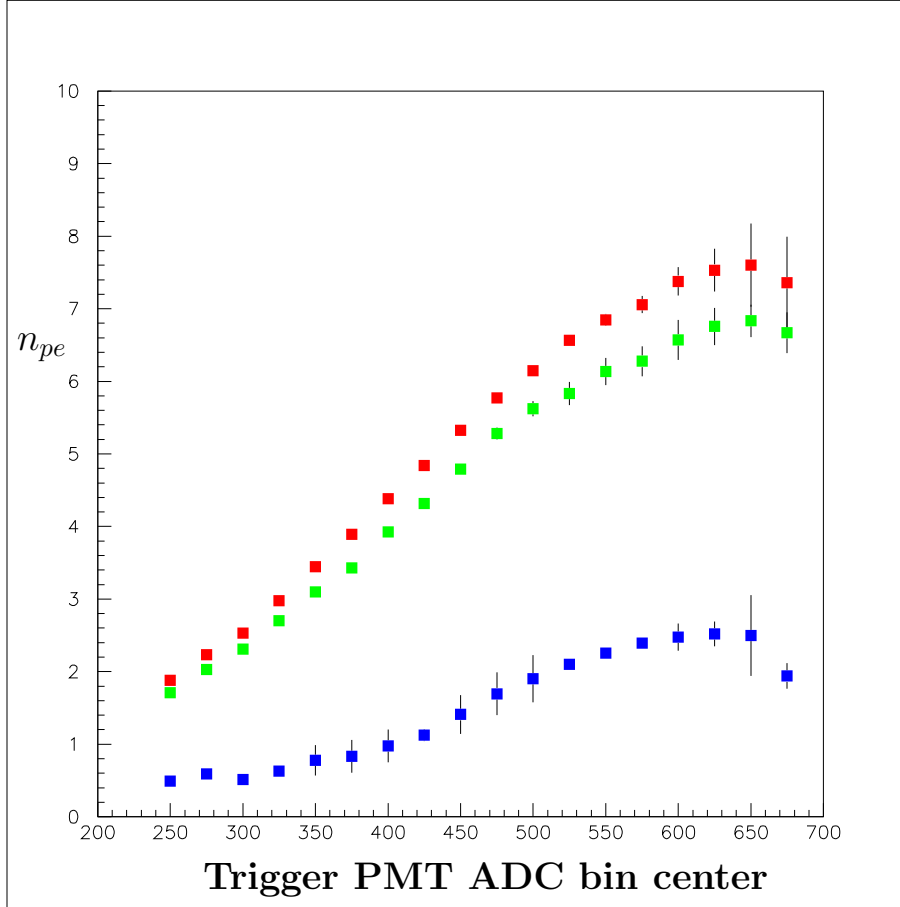
Figure 17: Dependence of the n_{pe}'s on the trigger PMT ADC channel. Closed squares are the n_{pe}'s for the FNAL extruded scintillator strip (red), Kharkov extruded scintillator strip (green), and ELJEN diamond cut strip (blue). Note that the FNAL and Kharkov scintillator strips have reflective coating, while ELJEN was only wrapped in the aluminized mylar.

were performed. In Fig. 19, the dependence of the measured number of photo-electrons versus the trigger PMT response for different HV settings for a tested R6095 are shown as closed squares. The green points are at $HV = 900$ V, the red points at $HV = 850$ V, and the blue points at $HV = 800$ V. The open squares correspond to the χ^2 distributions of the fits. The maximum difference in estimated number of photo-electrons for the extrapolated end point is $< 10\%$.

Measurements were made with cosmic ray muons in order to verify the above results. The light yield for R6095 PMT with FNAL scintillator and 1 mm diameter single clad Y11 fiber was determined. As a gate for ADC the coincidence of the trigger PMT and the scintillator counter positioned above the scintillator strip was used. The counter had 1 cm thick, 1.5×4 cm^2 scintillator. A fit to the test PMT spectrum, selected with a cut on the trigger PMT ADC
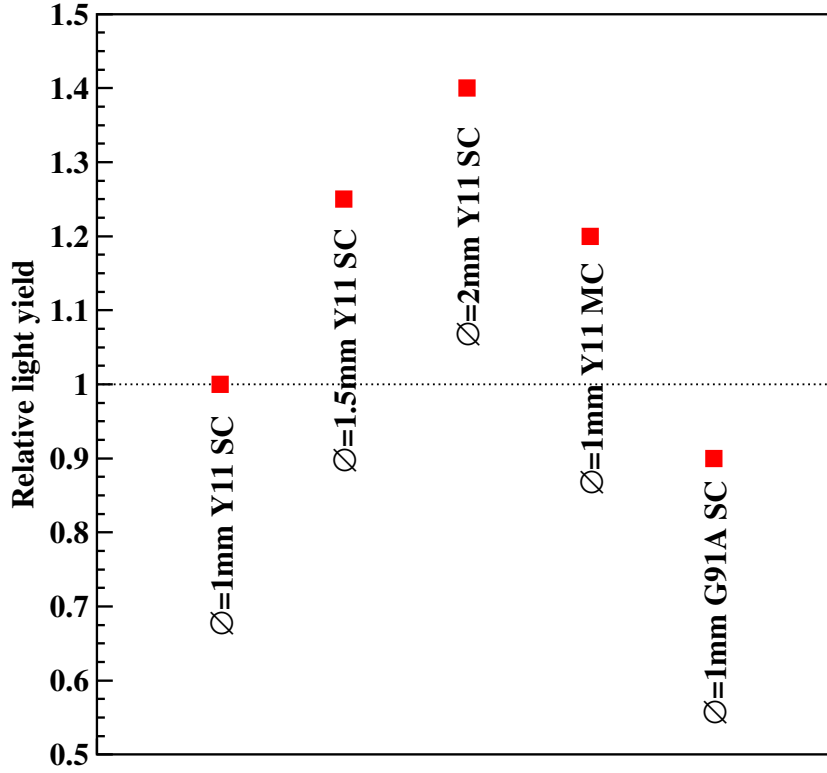
Figure 18: Light yield for different WLS fiber readout relative to 1mm diameter, single clad Y11 fiber. In all cases the fibers were glued to the FNAL extruded fiber and the HAMA-MATSU R7899 PMT was used for the readout.

in the range of MIP energy deposition, yielded ~ 9 photo-electrons. There is a difference of 20% compared to the number of photo-electrons obtained with ^{90}Sr source (~ 2 MeV energy deposition). This difference can be explained by the fact that in the cosmic setup the average path of particles is > 1 cm as well as the energy loss in the 1mm titanium dioxide coating that would lower β energy deposited but not influence the cosmic ray muon energy deposition. More precise measurements of the absolute photo-electron yield will be done with a box-prototype (see below).

5.6   Multiple fiber readout

In the final design of the PCAL, each scintillator strip will be read out with three WLS green fibers embedded in the grooves on the surface of the scintillator strip. To estimate the expected light yield for three fiber readout, the Amcrys-Plast, Kharkov, extruded scintillator strips with three grooves were used with KURARAY 1 mm diameter, single clad Y11 fibers. In Fig. 20, the light yield dependences on the trigger PMT ADC bin center are shown for one,
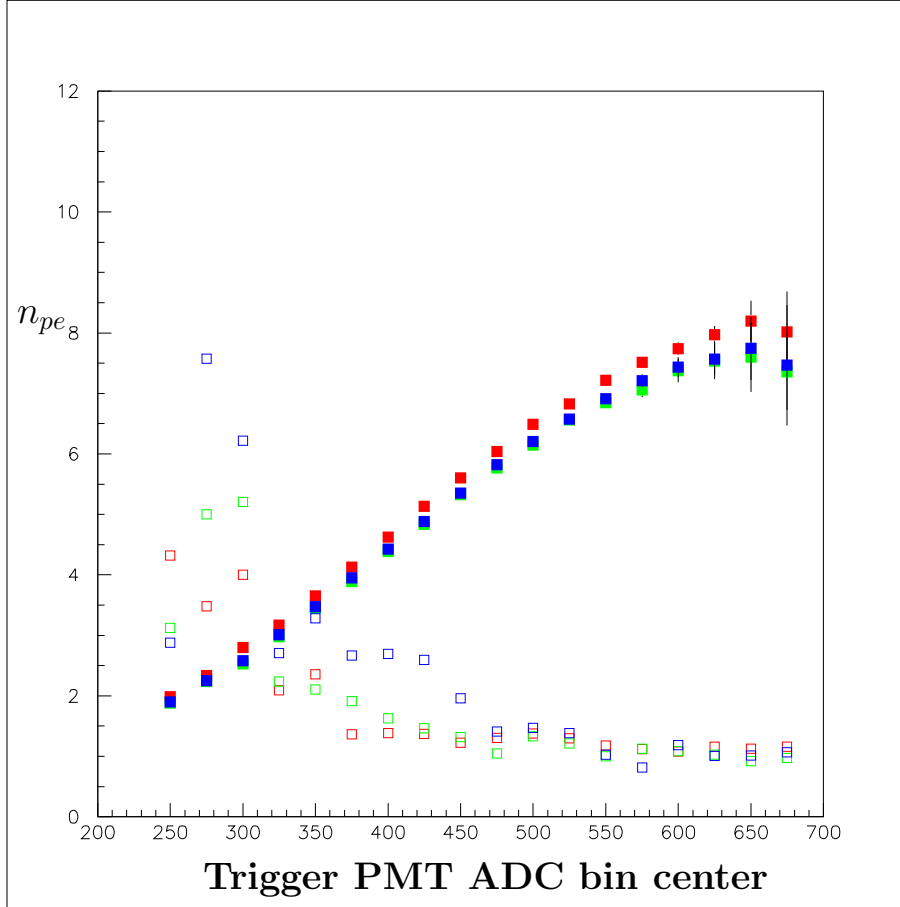
Figure 19: Light yield for the HAMAMATSU R6095 PMT operated at different HV settings. The blue squares correspond to $HV = 800$ V, the read squares are at $HV = 850$ V, and the green squares $HV = 900$ V. The open squares correspond to the χ^2 distributions of the fits.

two, and three fiber readout with closed squares, upward closed triangles, and downward closed triangle, respectively. Source (^{90}Sr) position was unchanged during these measurements. As one can see the number of photo-electrons is proportional to the number of fibers. In the figure the open squares represent the χ^2 distribution for the fit to two fiber readout case.

Source position dependence was studied using three fiber readout. Source was moved on the surface of the strip from one side to another and the measurements of the light yield were performed at four points. The results are shown in Fig. 21. No dependence on the position of the source is observed. However, it should be noted that the multi fiber readout and the position dependence should be checked with final strip geometry, since the Kharkov scintillators are only 2.63 cm wide, while for the pre-shower 4.5 cm wide scintillators will be used.
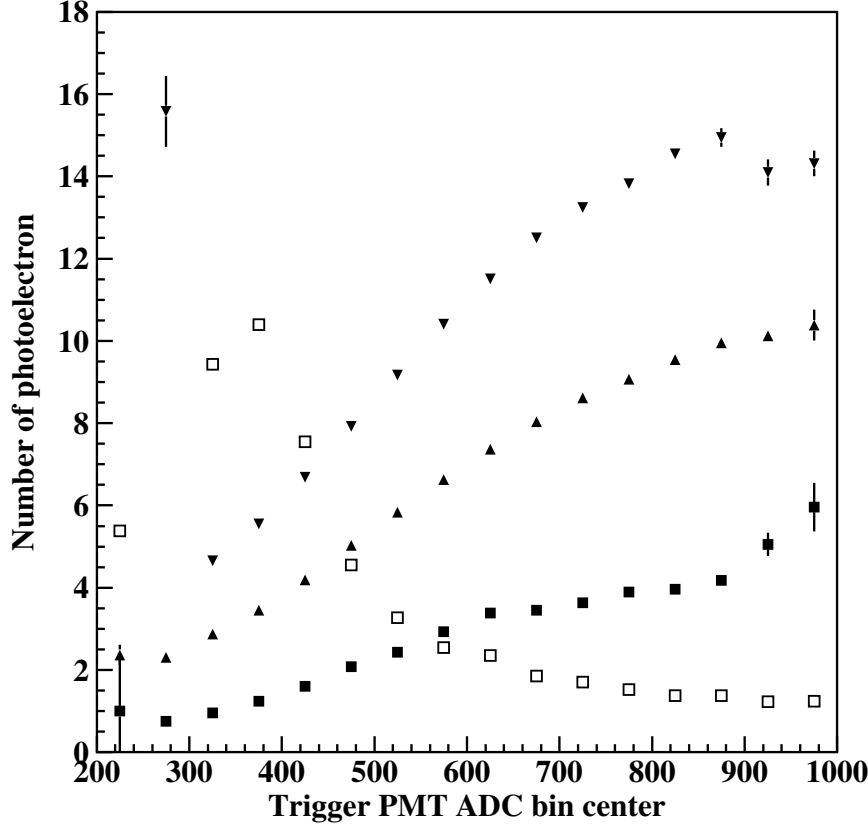
Figure 20: Dependence of the n_{pe}'s on the trigger PMT ADC channel for one (closed squares), two (closed upward triangles), and three (closed downward triangles) WLS fiber readout from Kharkov scintillator strip with three grooves on the surface. Radiative source was ^{90}Sr and the readout PMT was the R6095. The open squares represent the χ^2 distributions for the fit to two fiber readout case.

5.7 Summary of the test measurements

Light yield for several different types of scintillator strips, WLS green fibers, and PMTs were measured. The purpose of these measurements were to select the best combination of the scintillator-WLSF-PMT based on the performance and price. Systematic uncertainties of the relative light yield measurements of different combinations of scintillator-WLSF-PMT were < 10%. For the absolute light yield, the estimated systematic uncertainty was $\sim 20\%$.

The best results were obtained with the FNAL extruded scintillator, KURARAY Y11 fibers, and the HAMAMATSU R7899EG PMT. The HAMAMATSU PMT R6095, selected with QE > 16% at 500 nm, showed only $\sim 25\%$ less light yield, while in price it is about 33%
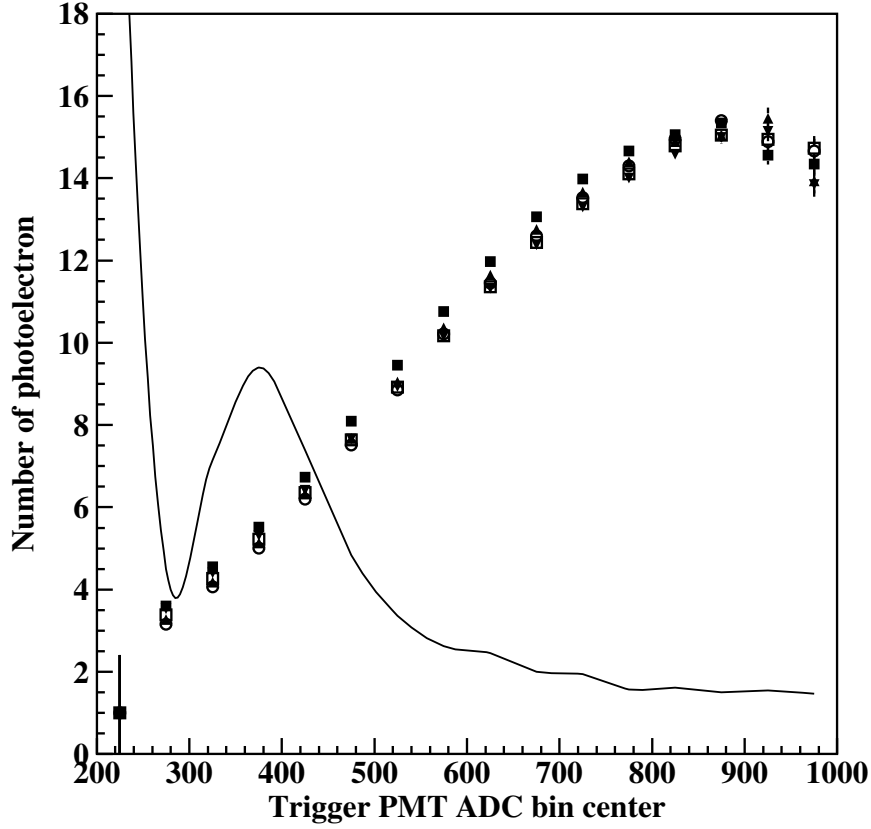
Figure 21: Dependence of the n_{pe}s on the trigger PMT ADC channel for three fiber readout of Kharkov three groove scintillator strip. Different color symbols correspond to different position of the ^{90}Sr radiative source. For light readout R6095 PMT was used.

times less expensive. Multi-clad fiber readout showed $\sim 20\%$ more light than a single clad fiber, but it is about 35% more expensive.

Based on the measurement results and the available price estimates, the choice for the pre-shower will be: the FNAL extruded scintillator, KURARAY 1 mm diameter, single clad Y11 fiber, and the HAMAMATSU R6095 PMT, selected with QE $> 16\%$ at 500 nm. It should be noted that by the performance and price, extruded scintillators from Amcrys-Plast, Kharkov (Ukraine), wave-length shifting fibers G91A from BICRON and the HAMAMATSU PMT R1450, selected to have $> 18\%$ quantum efficiency at 500 nm, were not too far from the best choice set and generally meet the requirements for the pre-shower.

Component	Optimal Choice
WLS Fiber	KURARAY 1 mm diameter, single clad WLS fiber (Y11)
Photomultiplier	HAMAMATSU R6095 PMT, selected with QE > 16% at 500 nm
Scintillator	FNAL extruded scintillator

Table 4: Final Choice for PCAL components

5.8   Planned Prototypes

Two stages of prototyping are now being considered. The first box-prototype is small and has been constructed from existing materials. The dimensions are on the order of 30 cm. Top and side views are shown below in Fig.22. The prototypes small size will allow the detector to be placed in the Hall-B beam for direct studies. Fifteen layers of scintillator and lead will be stacked with horizontal supports to secure the layers. Openings in these supports will allow the WLS fibers to be brought out of the stack and guided to photomultiplier tubes. Layers will be read out on three sides so as to mimic the final UVW readout planned for the PCAL. Three layers comprise a module. The full five module longitudinal depth of the box-prototype should allow accurate characterization of the shower and a fairly complete determination of the combined response of the components both in terms of energy and timing. The optimal scheme for routing the fiber is still under discussion. The plan is to follow a design that would work for the final calorimeter. Space constraints and maintenance access are important for the placement of the photomultiplier tubes as well as the mechanism that holds and couples the fibers to the photomultiplier tubes. The proposed fibers, scintillator, and photomultipliers listed in table for the final PCAL will be used.

A second stage prototype, a full scale version, will be critical for exploring other construction, quality control and testing challenges. The full-scale prototype should match the dimensions for the final PCAL. The construction of at least part of a full scale prototype will provide focus for support, alignment, and assembly demands. The details of the component storage, delivery and alignment can be studied. Methods for supporting and stacking the elements during the construction phase and the methods for fiber handling, gluing and routing can be studied. The properties of the components for the largest dimensions can be characterized. Critical aspects of the design such as attenuation lengths can be studied and methods for measuring these characteristics can be incorporated into the final assembly plans. The large number of photomultipliers, scintillator strips, the significant length of fiber and
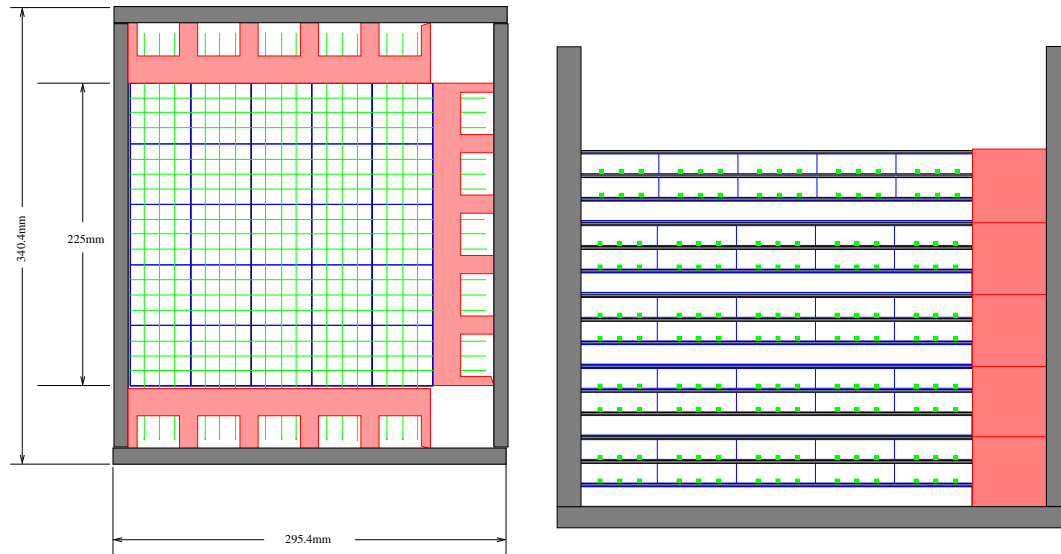
Figure 22: Two views of the box prototype currently under construction. The full 5 module longitudinal depth will allow study of the behavior of shower development and actual sampling features.

the length of the longest pieces create challenges that can be best addressed by building at least partially a full scale prototype.

6   Construction

Construction of the PCAL consists of several quasi-independent processes. Each process requires independent man power and work space. Most of these processes require clean environment. Handling of many items, such as scintillator strip, fibers, μ-metal shield, lead, PMTs etc., requires use of gloves. Below are the steps/processes involved and resources needed in the construction of the PCAL -

1. Preparation of scintillator strips with WLS fibers

   Requires semi-clean area with a 4.5 meters long table and open shelves for about 3000 meters of scintillator strips. Table should be instrumented with fixtures for gluing. Process requires tools for measuring dimensions and tools for cutting and gluing optical fibers. Preparation of the scintillator-fiber assembly will be done for one sector at a time. Work will include:

- visual inspection of scintillator strips

- cut the strips to the correct length, measure dimensions

- cut and inspect fibers

- gluing fibers into grooves

- inspection of the gluing quality

2. Assembly and test of PMTs and dividers

Requires a room with dark box and storage shelves. Process requires tools for mechanical assembly, oscilloscope, HV system for PMTs, cables, electronics and DAQ. Assuming that divider components are ready. Work will include:

- assembly of dividers to the end cups of the PMT housing

- assembly of the PMT housing, cleaning plastic tubes and end-cups, installation of μ-metal shield

- full assembly of the PMT, divider and housing system

- measurement of the relative sensitivity to the green light (500 nm) and gain of each PMT using a photo-diode, compare with specifications

3. Stacking of the scintillator and lead layers

Requires semi-clean, 8×8 m^2 room. Room should have access to an overhead crane, or other lifting device to move lead sheets. Process will require wide paper or Teflon sheets to place between lead and scintillator layers. Stacking will be done one sector at a time. Work will include:

- cleaning and assembly of the back plate and the side walls of the box

- stacking scintillator and lead layers

- after scintillator layer is in place, put fixtures and shims to secure position of the scintillator layer from all sides, cover the layer with paper or Teflon sheets, put the lead sheet

- after all layers are stacked, put enough paper or Teflon sheets on top of the last layer to have tight, uniform compression of the scintillator-lead layers between the two end plates

- put the front plate and bolt it to the side walls

- inspect that all fibers are in place, there are no broken fibers

- move the PCAL module where high load crane is available and rotate it to have front plate down

- move the module to the area where PMTs will be assembled

Plate that holds the weight of the PCAL should have strong back support to prevent bowing. There should be at least two strong backs, one for stacking and second for the PMT assembly.

4. Mounting of fiber-adapters and PMTs

   Requires semi-clean 6×6 m^2 room, gluing fixtures, polishing instruments, black masking tape, tools for mechanical assembly, oscilloscope, HV power supply, and HV and signal cables. Work will include:

   - mount shelves and fiber-PMT adapters

   - position fibers inside the adapters according to the readout channel distribution and glue them

   - cut and polish the ends of the fibers

   - clean shelves and adapters

   - mount aluminum sheet covers

   - mount PMTs

   - check for light leaks, if there are light leaks use black masking tape to cover

   - move the PCAL module to the test area

5. Test of the PCAL module with cosmic particles

   Requires about 6×6 m^2, air conditioned area, cables and electronics for one module, working DAQ system. Work will include cabling, checking each channel, data taking, and analysis.

7 Collaboration

Several institutions are involved in the design, prototyping and construction of the PCAL. The main contributions by these institutions will be in man power needed for the per-design simulations, for the design, testing, and prototyping. In the construction stage individual institution can take over of separate tasks or participate in different activities. The main players are:

- Yerevan Physics Institute (YerPhI), will provide scientists experienced in the detector design, construction, and simulation, as well as students to help during the assembly and test of the PCAL modules. It is expected also that some parts needed for the prototyping and construction can be made at YerPhI facilities (e.g. adapters for the fiber-PMT connection). YerPhI collaboration already made significant contribution in the simulations, design, and prototyping of the PCAL.

- James Madison University (JMU), will provide scientists and students to participate in the design, prototyping, and construction of the PCAL. JMU group already made significant contribution to the testing of the PCAL components.

- Institut de Physique Nucleaire d'Orsay (INP), will provide engineers to participate in the design of the PCAL. INP group already made significant contribution to the design of the PCAL.

- Ohio University (OU), will provide scientists and students to participate in the design, prototyping, and construction of the PCAL. OU group already made contribution to the design of the PCAL components.

- Norfolk State University (NSU), will provide scientists and students to participate in the prototyping and construction of the PCAL.

- Jefferson Lab (JLAB), will manage the project, will lead the design, prototyping, and construction of the PCAL. Will provide infrastructure for the project, work space for different activities, and engineering and technical help.

References

[1] M. Amarian *et al.*, NIM **A 460**, 239 (2001),

[2] N. Dashyan and S. Stepanyan, CLAS-Note 2007-001,

[3] K. Whitlow, N. Dashyan and S. Stepanyan, CLAS-Note 2007-002.

[4] G. Asryan, H. Voskanyan, and S. Stepanyan, CLAS-Note 2007-007.

[5] N. Dashyan and S. Stepanyan, CLAS Note 2006-016.

[6] Ph. Rosier, Preliminary Finite Element Analysis of the Preshower Calorimeter for the CLAS12 .

[7] S. Stepanyan *et al.*, CLAS-NOTE 2002-001 (2002).

[8] MINOS Far detector, arXiv:hep-ex/0507018 (2005).

[9] FNAL Extruder http://www.nicadd.niu.edu/research/extruder.

[10] M. Amarian *et al.*, CLAS-NOTE 1992-012 (1992).

[11] V. Burkert *et al.*, CLAS-NOTE 1992-008 (1992).

[12] K. Giovanetti and A. Stavola, Fiber adapters for pre-shower tests (JMU).

[13] HBOOK, Statistical Analysis and Histogramming, CERN program library long write-ups Y250.

[14] Physics Analysis Workstation, CERN program library long write-ups Q121.